Cellular Signalling 83 (2021) 109994

Contents lists available at ScienceDirect

Cellular Signalling

journal homepage: www.elsevier.com/locate/cellsig

Extracellular vesicles produced by primary human keratinocytes in response to TLR agonists induce stimulus-specific responses in antigen-presenting cells

Christopher J. Papayannakos [a,*,1], James A. DeVoti [b,c], Mohd Israr [b], Habeeb Alsudani [d], Vincent Bonagura [b,c], Bettie M. Steinberg [b,e]

[a] Donald and Barbara Zucker School of Medicine at Hofstra/Northwell, 500 Hofstra University, Hempstead, NY 11549, USA
[b] The Institute of Molecular Medicine, The Feinstein Institutes for Medical Research, 350 Community Drive, Manhasset, New York, USA
[c] Department of Pediatrics, Steven and Alexandra Cohen Children's Medical Center of New York, Barbara and Donald Zucker School of Medicine at Hofstra/Northwell, Hempstead, NY, USA
[d] Cold Spring Harbor Laboratory, Cancer Center, Cold Spring Harbor, New York, USA
[e] Department of Molecular Medicine, Barbara and Donald Zucker School of Medicine at Hofstra/Northwell, Hempstead, NY, United States of America

ARTICLE INFO

Keywords:
Extracellular vesicles
Keratinocytes
Langerhans cells
Cytokine
LC3b-II
Toll-like receptor
Autophagy

ABSTRACT

Cells can communicate through the extracellular vesicles (EVs) they secrete. Pathogen associated molecular patterns (PAMPs), alter the biophysical and communicative properties of EVs released from cells, but the functional consequences of these changes are unknown. Characterization of keratinocyte-derived EVs after poly (I:C) treatment (poly(I:C)-EVs) showed slight differences in levels of EV markers TSG101 and Alix, a loss of CD63 and were positive for autophagosome marker LC3b-II and the cytokine IL36γ compared to EVs from unstimulated keratinocytes (control-EVs). Flagellin treatment (flagellin-EVs) led to an EV marker profile like control-EVs but lacked LC3b-II. Flagellin-EVs also lacked IL-36γ despite nearly identical intracellular levels. While poly(I:C) treatment led to the clear emergence of a > 200 nm diameter EV sub-population, these were not found in flagellin-EVs. EV associated IL-36γ colocalized with LC3b-II in density gradient analysis, equilibrating to 1.10 g/mL, indicating a common EV species. Poly(I:C), but not flagellin, induced intracellular vesicles positive for IL-36γ, LC3b-II, Alix and TSG101, consistent with fusion of autophagosomes and multivesicular bodies. Simultaneous rapamycin and flagellin treatment induced similar intracellular vesicles but was insufficient for the release of IL-36γ^{+}/LC3b-II^{+} EVs. Finally, a qRT-PCR array screen showed eight cytokine/chemokine transcripts were altered ($p < 0.05$) in monocyte-derived Langerhans cells (LCs) when stimulated with poly(I:C)-EVs while three were altered when LCs were stimulated with flagellin-EVs compared to control-EVs. After independent confirmation, poly(I:C)-EVs upregulated BMP6 ($p = 0.035$) and flagellin-EVs upregulated CXCL8 ($p = 0.005$), VEGFA ($p = 0.018$) and PTGS2 ($p = 0.020$) compared to control-EVs. We conclude that exogenous signals derived from pathogens can alter keratinocyte-mediated modulation of the local immune responses by inducing changes in the types of EVs secreted and responses in antigen presenting cells.

1. Introduction

Keratinocytes are considered an integrated part of the innate immune system, with constant exposure to exogenous stresses such as invading microbes [1–4]. Covering most epithelial surfaces, they have evolved the ability to detect pathogen associated molecular patterns (PAMPS) through the expression of specific sets of receptors, including select Toll-like Receptors (TLR) [4–9]. Upon TLR-ligand engagement, keratinocytes synthesize cytokines and chemokines that not only promote inflammation but communicate with local immunocytes, including the epithelial-resident immature dendritic cells, Langerhans cells (iLCs). Extracellular vesicles (EV) are an emerging paradigm for cell-cell communication, especially among cells of the immune system [10]. How EV populations from keratinocytes change and how their signaling

* Corresponding author at: The Feinstein Institutes for Medical Research, 350 Community Drive, Manhasset, NY, USA.
E-mail address: cpapayanna@northwell.edu (C.J. Papayannakos).
[1] Current address: The Institute of Molecular Medicine, The Feinstein Institutes for Medical Research, 350 Community Drive, Manhasset, New York, USA.

https://doi.org/10.1016/j.cellsig.2021.109994
Received 23 December 2020; Received in revised form 23 March 2021; Accepted 24 March 2021
Available online 27 March 2021

potential is altered during the initial innate immune response is not well understood.

EVs vary in their physical and biological properties and in the cargo molecules they carry [11–14]. Recent reports show that cytokine-loaded EVs are often released from cells and innate immune signaling can alter this [14,15]. Human foreskin keratinocytes (HFKs) express a subset of the TLRs including TLR-3 and TLR-5 [4,9]. Activation of TLR-3, recognizing primarily endocytosed double-stranded RNA (including synthetic poly(I:C)) and TLR-5, recognizing extracellular bacterial flagellin, both lead to cytokine induction and release in keratinocytes [16]. The IL-1 family member IL-36γ, is a cytokine made predominantly by epithelial cells and can be induced and secreted from human keratinocytes in response to TLR3 and TLR-5 agonists [17–19]. Our group previously reported that IL-36γ is released in complex with an unknown EV species by an unknown mechanism when HFKs are stimulated with poly(I:C) [16].

EV populations are heterogenous by nature and it is important to understand and describe subpopulations that may arise, potentially influencing the message EVs send during immune responses. Classical exosomes are EVs derived from multivesicular bodies (MVBs), but EVs derived from other intracellular membranes are becoming recognized as important contributors to cell-cell communication and unconventional protein secretion. In particular, autophagosome-derived EVs result from the fusion of the organelle with the plasma membrane or through interactions with MVBs, giving rise to non-exosomal, small EV species with select cargos [15,20,21]. Autophagy is a broad term used to describe catabolic cellular processes that recycle damaged organelles, mitigating stresses attributed to starvation or infection. A central event defining autophagosome biogenesis is the lipidation and cleavage of cytoplasmic Microtubule Associated Protein 1 Light Chain 3 Beta (MAP1LC3B; henceforth referred to as LC3b), —I to LC3b-II [22,23]. Canonically, the fate of the autophagosome is fusion to the lysosome for cargo degradation. Autophagosomal-multivesicular body crosstalk and subsequent cargo release in the form of non-exosomal, small EVs has recently been recognized [15,20,24]. There is growing evidence in the literature that autophagosomal-MVB crosstalk may lead to an exosome-like subpopulation of EVs bearing the autophagosomal membrane, and atypical EV marker, LC3b-II [25,26]. Release of LC3b-II^{+} EVs, a hallmark of this process, has not been reported in primary human keratinocytes.

To better understand cell-cell communication during the initial stages of infection, we asked if TLR-activation altered the types of EVs secreted by keratinocytes and whether these EV populations could transmit TLR-specific information to local antigen presenting cells. We found that activation of TLRs differentially modifies the pathway for EV generation and cargo selection and leads to TLR/EV-specific gene expression changes in monocyte-derived iLCs. We conclude that EVs in epithelia can transmit information that is specific to the type of microbial threat, to aid in mounting a targeted immune response.

2. Materials and methods

2.1. Cell culture and stimulation

Human keratinocytes (HFKs) were isolated from discarded neonatal foreskins as described previously [27]. Use of these keratinocytes was approved as “Exempt” by the Feinstein Institutional Review Board. All experiments were performed on pools of HFKs representing between 4 and 6 individuals. HFKs were co-cultured with growth-arrested J2-3t3 fibroblasts until sub-confluent in *E*-media containing 10% Fetal Clone-II (Hy-Clone) and growth factors [27]. J2-3t3 feeder cells were removed with EDTA and gentle agitation prior to media conditioning by HFKs. HFK stimulations were performed in *E*-media supplemented with growth factors and 1% Fetal Clone-II (Hy-Clone) that was exosome-cleared by ultracentrifugation at 100,000 xG for 18 h. Cells were stimulated with 1.5 μg/mL high-molecular weight polyinosinic-polycytidylic acid (poly (I:C)) (Invivogen) or 1 μg/mL flagellin (from *S. typhimurium,* Invivogen) for the times indicated. For induction of autophagy, HFKs were co-stimulated with 1 μM rapamycin (Sigma) and 1 μg/mL flagellin, and re-dosed with additional rapamycin at 24 h.

2.2. Western blotting

Whole cell lysates were prepared by lysing HFKs on ice for 40 min in 1× Tris-EDTA buffer with 1% NP40 Alternative (Millipore), containing protease and phosphatase inhibitors (Roche). Insoluble protein and membranes were pelleted by centrifugation at 20,000 xG for 30 min at 4 °C. Total protein in lysates was measured by BCA assay (ThermoFisher), separated through 4–20% TGX gradient gels (Bio-Rad), electrotransferred onto PVDF membranes (Millipore), and blocked in BSA blocking buffer (Li-Cor) at room temperature for one hour. Membranes were probed overnight for Alix (Bio-Rad), TSG101 (Abcam), LC3b (Thermo-Fisher), IL36γ (R&D), CD63 (Bioss) or β-actin (Sigma). Membranes were then washed, probed with near-infrared dye-conjugated secondary antibodies donkey anti-mouse CW800, donkey anti-rabbit CW800, or donkey anti-goat 680RD (Li-Cor). Blots were scanned and quantified using Azure Biosystems Sapphire Biomolecular imager.

2.3. Extracellular vesicle preparation

This work utilizes the term EV to represent the small extracellular vesicles that pellet from cell-conditioned media after ultracentrifugation at 100,000 xG. This material likely consists of a heterogenous population of EVs including exosomes and microvesicles. EV enrichment was adapted from an exosome isolation protocol by ultracentrifugation of conditioned cell culture media [28]. Approximately 36 mL of conditioned media from approximately 2×10^7 HFKs was collected after 48-h stimulations and centrifuged at 400 xG for 5 min followed by 2000 xG for 15 min. Clarified conditioned media was then kept at −80 °C until EV processing. To prepare EV pellets, conditioned media was thawed on ice and then ultra-centrifuged for 60 min at 20,000 xG, in an AH-629 rotor (Sorvall), the supernatant transferred to a new tube and spun for 90 min at 100,000 xG (100 k pellets). Crude pellets were washed by resuspending in ice cold PBS and re-pelleted at 100,000 xG for 90 min in a TH-641 rotor (Sorvall). Pellets were recovered in about 100 μL 1× PBS. Equal volumes were mixed with 6× denaturing loading buffer prior to western blotting or were kept at 4 °C for protein measurement and LC stimulation experiments. Isolated 100 k pellets were never frozen.

2.4. Density gradient centrifugation of EVs

EV density gradient protocol was adapted from Jeppesen et al. 2019 [21]. Total crude 100 k pellets were collected in approximately 100 μL 1× PBS, adjusted to 40% Opti-prep (Millipore Sigma) and placed at the bottom of a 5 mL ultra-centrifuge tube (Thermo Scientific). Discontinuous gradients were formed on top of samples by layering equivalent volumes of Opti-prep, from 35% to 0%, in 5% increments. 50% Opti-prep working stock was diluted with Solution B (0.85% NaCl, 10 mM Tricine-NaOH, pH 7.4) to prepare gradient solutions. Gradients were centrifuged for 18 h in an AH-650 rotor (Sorvall) at 100,000 xG at 4 °C. 12 equivalent volume fractions were taken from the top, excluding the bottom original sample material. Refractive indices were measured with 20 μL of each fraction using a refractometer (Sper Scientific), then diluted with ice cold 1× PBS to 4 mL and centrifuged for 60 min at 100,000 xG. Resulting pellets were collected and boiled in 6× loading buffer for 5 min and analyzed by western blot.

2.5. Subcellular fractionation

HFK monolayers growing in 150 mm plates were stimulated as indicated for 24 h. Cells were washed 3 times with ice cold 1× PBS and gently lifted from plates using a cell scraper under ice cold, 1× PBS.

Monolayers were pelleted at 500 xG for 5 min at 4 °C and resuspended in 0.5 mL lysosome enrichment buffer-A (Fisher) containing Mini-complete protease (Roche) and PhosSTOP phosphatase (Roche) inhibitors at 1:100. Cells were Dounce-homogenized on ice in the absence of detergents, prior to adding 0.5 mL lysosome enrichment buffer-B (Fisher). Homogenates were centrifuged at 4000 xG for 20 min and then clarified again at 7000 xG for 20 min at 4 °C. Approximately 1000 μg of protein from clarified homogenates were adjusted to 40% Opti-prep with 50% Opti-prep working stock. Sample was laid in the bottom of a 5 mL ultracentrifuge tube (Thermo Scientific) and discontinuous gradients were formed, and samples centrifuged as described above for EV isolation. Equal volume fractions were recovered by hand from the top of the gradients. For each fraction, density was measured, diluted, centrifuged and subject to western blot analysis as described above.

2.6. Transmission electron microscopy and size distribution

Washed pellets of EVs derived from conditioned media from approximately 6.0×10^7 control, poly(I:C)-stimulated or flagellin-stimulated HFKs were fixed in 2.5% glutaraldehyde in 0.1 M sodium cacodylate (pH 7.4) at 4 °C overnight. Pellets were washed in 0.1 M sodium cacodylate at room temperature. 4% molten agarose was added to pellets, centrifuged at 1000 xG for 10 min at 30 °C, then chilled in ice until solid. 1.0 mL of 1% osmium tetroxide solution was added for 1 h at room temperature. After washing, samples were dehydrated in a graded ethanol series (50%, 60%, 70%, 80%, 90% 100%) for 10 min each. Samples were then embedded in 812 EMed resin, sectioned at 60–90 μms in an ultramicrotome and imaged on an H 7000 Hitachi Transmission Electron Microscope. A total of four diameter measurements were made on each visible EV structure on scaled micrographs with imageJ. Diameters were sorted into 10 nm bins and distribution plotted and expressed as probability density functions using R statistical software.

2.7. Langerhans cell stimulation

Immature Langerhans cell-like cells (iLCs) were generated from monocytes isolated from peripheral blood mononuclear cells (PBMC) from three healthy donors as described previously [29,30]. Use of human monocytes was approved by the Feinstein Institutional Review Board with consent obtained for each donor. Protein concentration of EV pellets was determined by BCA assay as a surrogate to standardize the EV-stimulus (Thermo Scientific). iLCs were resuspended at 1×10^6 in serum-free RPMI and incubated with 8.0 μg EV pellet protein, isolated from 2×10^7] poly(I:C)-stimulated, flagellin-stimulated or control HFKs. Each donor's iLCs were treated with control-EVs, poly(I:C)-EVs, flagellin-EVs or left unstimulated for 8 h at 37 °C with gentle agitation. This represented an approximate HFK:iLC ratio of 20:1, not dissimilar to that reported by Bauer et al., 2001 [31].

2.8. Transcript arrays and qPCR

Total RNA was isolated from the iLCs with the High Pure RNA isolation kit (Roche) and cDNA libraries were generated using RT^2 First Strand Kit (Qiagen) as per manufacturer's instructions. Each iLC cDNA library was amplified on RT^2 Profiler: Human Cytokine and Chemokine PCR arrays (Qiagen). All RNA and cDNA samples were free of genomic DNA contamination and passed manufacturer's QC parameters for analysis. Briefly, ΔC_T was calculated using averaged threshold cycles of the 5 housekeeping genes: *Beta Actin (ACTB), Beta-2-Microglobulin (B2M), Glyceraldehyde-3-Phosphate Dehydrogenase (GAPDH), Hypoxanthine Phosphoribosyl transferase 1 (HPRT1),* and *Ribosomal Protein Lateral Stalk Subunit P0* (*RPLP0*) according to Qiagen's GeneGlobe analysis software and averaged across donors prior to normalization of EV-stimulated LCs to unstimulated LCs. Transcript levels 1000-fold lower than GAPDH under either unstimulated or stimulated conditions, were disregarded for interpretation and were considered as biologically meaningless.

Independent confirmation of the five significantly elevated transcripts was carried out using probe-based qPCR with primers/probes for CXCL8 (Hs00174103_m1), CCL3 (Hs00234142_m1), VEGFA (Hs00900055_m1), CXCL16 (Hs00222859_m1), BMP6 (Hs01099594_m1), and GAPDH (Hs01922876_u1) for normalization, all purchased from Applied Biosystems/Life Technologies. To measure COX-2 induction, *PTGS2* transcript was measured by qRT-PCR using intron-spanning primers/probe against Hs00153133_m1 (Applied Biosystems/Life Technologies). *IL-36γ* transcript was measured using primers/probe as previously described [29]. Amplification was performed on an Applied Biosystems 7900 HT with the iScript One-Step RT-PCR kit (Bio-Rad). Total RNA was reverse transcribed at 50 °C for 10 min, followed by 5 min at 95 °C. Amplification was performed for 40 cycles of 95 °C for 15 s and 60 °C for 1 min. Averaged Ct values were compared to Ct values of *GAPDH* as a housekeeping gene for ΔCt determination.

2.9. Statistical analysis

Significance of difference for qPCR arrays was determined by Student's *t*-test using Qiagen's GeneGlobe platform, with each transcript normalized to manufacturer's recommended housekeeping genes. Non-linearized expression data compared unstimulated iLCs to control-EV stimulated iLCs, and poly(I:C)- and flagellin-EV stimulated iLCs to control-EV stimulated iLCs. Changes in transcript levels that showed greater than 2-fold with stimulation with a p-value <0.05 were considered significant and were included for confirmation. Individual, two-tailed paired, Student's *t*-tests were performed on qPCR confirmation measurements. The difference in EV size distribution, as measured by EM was determined by multiple Kolmogorov-Smirnov tests and accepted as significant where p-value <0.05. The Student's two-tailed, paired t-test was used for the qPCR of *COX-2* induction and for analysis of densitometry measurements on western blots; $p < 0.05$ was considered significant.

3. Results

3.1. Shifts in EV markers and size distribution indicate TLR-agonist dependent genesis of disparate EV populations

We began our comparison of the properties of poly(I:C)- and flagellin-stimulated HFK-derived EVs by characterizing the total EV populations, asking if EVs derived from stimulated HFKs showed differences in the levels of EV biomarkers CD63, Alix and TSG101 [32]. EV marker Alix changed very little with either poly(I:C) or flagellin treatment and was used to approximate relative differences in CD63 and TSG101 (Fig. 1a). There was a two-fold increase in TSG101 with the concurrent loss of CD63, approximately 80%, in the poly(I:C)-EVs (Fig. 1a). These results reflect changes specific to the EV populations, not intracellular levels which remained unchanged (Fig. 1b). As we previously reported, IL-36γ is present as EV cargo after its induction with poly(I:C) (Fig. 1c) [16]. Surprisingly, IL-36γ was absent from flagellin-EVs (Fig. 1c) despite nearly equivalent intracellular levels (Fig. 1d). This observation suggested a selective differential vesicular secretion mechanism activated by poly(I:C) and not flagellin, independent of the presence of the cytokine itself. Supporting this, the autophagy marker LC3b-II was markedly elevated in poly(I:C)-EVs, with only trace amounts detected in flagellin-EVs (Fig. 1c), suggesting formation of an autophagosome-derived EV population in poly(I:C) stimulated cells. Intracellular levels of LC3b-II in total cell lysates from the same parental cells were barely visible, although the cytosolic precursor LC3b-I was readily detectable, and the LC3b-II/LC3b-I ratio was significantly higher after poly(I:C) treatment compared to flagellin treatment (Fig. 1d). Thus, poly(I:C) stimulation affected autophagy more than stimulation

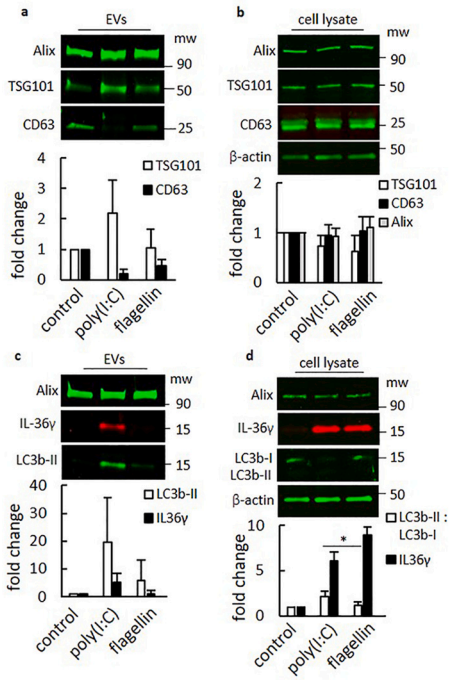

Fig. 1. Stimulation of TLR-3 but not TLR-5 induces the release of IL-36γ$^+$/LC3b-II$^+$ extracellular vesicles from normal keratinocytes. a) Representative western blot of EV pellets derived from 48-h TLR-stimulated or control HFK-conditioned media. Bars show mean fold-change ± SD in TSG101 and CD63 normalized to Alix, relative to untreated HFK pellets. $n = 3$ independently isolated EV pellets. b) Western blot of total intracellular protein from HFKs that produced the EVs shown in A. Bars show mean fold-change ± SD in TSG101, CD63 and Alix expression, normalized to β-actin, relative to untreated HFKs. $n = 3$ experiments. c) Western blot of total EV pellets derived from 48-h TLR-stimulated HFK-conditioned media. Bars show mean fold-change ± SD of IL-36γ and LC3b-II levels, normalized to Alix, relative to untreated HFK pellets. n = 3 independently isolated EV pellets. d) Western blot of total protein from HFKs that produced the EVs shown in C. Bars show the mean fold-change ± SD in LC3b-II:LC3b-I ratios and IL-36γ expression, normalized to β-actin, relative to untreated HFKs. n = 3 experiments. * $p < 0.05$ Student *t*-test. mw: molecular weight, EV: extracellular vesicles.

with flagellin, strengthening the idea that autophagy plays a role in poly (I:C) mediated EV generation.

Since the levels of markers and cargo molecules differed between EV populations, we asked whether the appearance and size distribution of EV populations were altered upon TLR-stimulation, visualizing isolated EV pellets by transmission electron microscopy. As expected, all three pellet preparations showed the presence of structures with the typical EV morphology (Fig. 2a, c, e). The majority of unstimulated-EVs were 60 to 100 nm in diameter, as indicated by the single prominent peak in its distribution (Fig. 2b). Flagellin-EV diameter distribution also showed a single prominent peak representing EVs with these diameters but with a slight right shift, indicating a broader distribution of larger EVs (Fig. 2d). Poly(I:C)-EVs did show a primary peak between 80 and 120 nm but in contrast to the other conditions, a second prominent peak representing EVs over 200 nm in diameter was evident (Fig. 2f), suggesting the selective generation of a unique sub-population of EVs with poly(I:C) stimulation. The distribution of each pellet was significantly different from each other (Fig. 2b, d, f), indicating a shift in the biogenesis of EVs in response to these TLR agonists ($p < 0.05 \times 10^{-8}$).

Density gradient separation followed by western blot analysis was used to determine whether the LC3b-II and IL-36γ markers were common to a specific species of EV and to measure the density of the unique sub-population of EVs present only after poly(I:C) stimulation. For poly (I:C)-EVs (Fig. 3a), Alix localized predominantly to fractions 6 and 7 with trace amounts in fractions 5 and 8, the density range reported for exosomes. LC3b-II localized specifically to fraction 7 with a density of 1.10 g/mL, indicating the externalization of a specific autophagosomal-derived EV subpopulation with a similar density to that reported for exosomes. IL-36γ co-localized strongly to the same fraction, supporting the presence of a common EV entity (Fig. 3a). Consistent with the bulk EV analysis, Alix also localized to fractions 6 through 8 with flagellin-EVs, but neither LC3b-II nor IL-36γ was detected (Fig. 3b).

3.2. The autophagosome plays a role in selective EV biogenesis and cytokine cargo incorporation

The density gradient analysis of poly(I:C)-EVs suggested that the IL-36γ cargo is complexed with an LC3b-II$^+$ EV. We asked if there was an intracellular association between IL-36γ and LC3b-II$^+$ membranes, as opposed to complexing in extracellular spaces post-release, using gradient separation of organelle-enriched keratinocyte homogenates. Twenty-four hours after poly(I:C) treatment, LC3b-II$^+$ autophagosomal membranes localized primarily to fractions 4 through 6 (1.08 to 1.10 g/mL) (Fig. 4a). This pool of organelles was also positive for the multivesicular body (MVB) markers TSG101 and Alix. A fraction of membrane-bound IL-36γ co-localized with these markers, strengthening the conclusion that IL-36γ is sequestered and taken up into the autophagosomal system. We compared this subcellular fractionation profile to that generated from an equivalent mass of flagellin-stimulated homogenates (Fig. 4a). Fractions 5 and 6 were positive for MVB markers Alix and TSG101 but were weakly positive for LC3b-II compared to the poly(I:C) homogenates. These fractions were negative for IL-36γ, suggesting that the parental compartment for the LC3b-II$^+$/IL-36γ$^+$ EV subpopulation was not readily generated during flagellin stimulation. The intracellular organelles from both poly(I:C)-treated and flagellin-treated keratinocytes that localized to higher density fractions 9 through 12 were negative for LC3b-II but did contain abundant IL-36γ, suggesting the cytokine is also located in other compartments of the *endo*-membrane system.

To determine whether autophagosome formation would lead to intracellular IL-36γ sequestration and secretion of LC3b-II$^+$/IL-36γ$^+$ EVs independently of poly(I:C) stimulation, HFKs were treated with rapamycin in combination with flagellin to induce autophagy. Again, flagellin alone induced no detectable LC3b-II and only trace amounts of IL36γ were present in the lower density fractions of intracellular organelles (Fig. 4b). Rapamycin plus flagellin induced formation of organelles positive for LC3b-II, and IL-36γ was now detected in these same fractions (Fig. 4b). These banding signatures point to the processing of LC3b-I to LC3b-II, its association with autophagosomal membranes and sequestration of IL-36γ, a pattern that resembles that seen with poly(I:C) treatment. Despite the induction of autophagy, treatment with flagellin plus rapamycin induced no increase in either LC3b-II or IL-36γ cargo in the EVs (Fig. 4c, d). This result suggests that sequestration of IL-36γ by autophagosomal membranes is necessary but not sufficient for its release in LC3b-II$^+$ EVs, and that the poly(I:C) is providing, either directly or indirectly, an additionally required signal.

3.3. EVs from keratinocytes treated with poly(I:C) and flagellin have divergent immune signaling potential

Monocyte-derived immature Langerhans-like cells (iLCs) were incubated with poly(I:C)-EVs, flagellin-EVs, control-EVs, or left unstimulated to determine whether EVs from HFKs altered the antigen-presenting cell immune response profile. All array data is shown in Supplementary Table 1. Our analysis showed that iLCs detect and respond to constitutively released control-EVs (Fig. 5a). Several of the transcript levels increased in iLCs by control-EVs represented proinflammatory genes, including members of the Tumor Necrosis Factor (TNF) signaling axis (TNF, TNFSF10 and TNFRSF1B), IL-7 and IL-11 (Fig. 5a). There were markedly divergent patterns in transcriptional

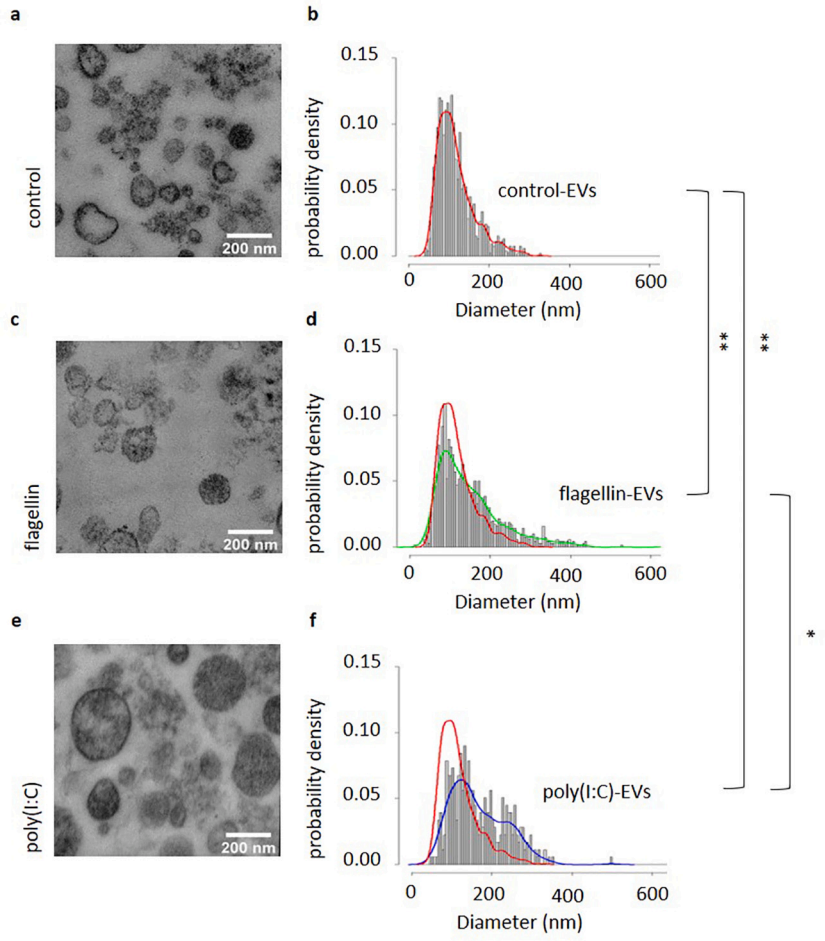

Fig. 2. TLR-3 stimulation but not TLR-5 stimulation induces generation of an EV sub-population with a larger diameter. (a, c, e) Transmission electron micrographs of total washed EV pellets derived from 48-h control, flagellin or poly(I:C)-stimulated HFK conditioned media, respectively. EVs displaying typical single membrane morphology were evident in all cases, with larger EVs prominent in the poly(I:C) sample. (b, d, f) Size distributions of EV diameters of control, flagellin- or poly(I:C)-stimulated HFKs, respectively, as determined by measurements of electron micrographs. Probability density functions are mapped on each histogram. Poly(I:C)-EVs (blue) or flagellin-EVs (green) functions are plotted over untreated control-EVs (red) diameters for comparison. Each probability density distribution was determined to be non-identical using Kolmogorov-Smirnov tests on single EV pellets. * $p < 0.5 \times 10^{-8}$; ** $p < 0.5 \times 10^{-16}$. EV: extracellular vesicles.

changes in cytokines and chemokines when iLCs were exposed to poly(I:C)- or flagellin-EVs compared to control-EVs (Fig. 5b, c). The differences in these responses are shown as relative expression in Fig. 5d. Compared to control-EVs, poly(I:C)-EVs significantly up-regulated CXCL16 and BMP6 while IL-16, IL-7 and TNFA transcripts were down-regulated. Transcript levels of these genes were not changed in response to flagellin-EVs. In contrast, flagellin-EVs induced the up-regulation of CCL3 and markedly increased CXCL8 transcripts. Neither CCL3 nor CXCL8 were altered by poly(I:C)-EVs. No transcripts were down-regulated after flagellin-EV stimulation. VEGFA was the only cytokine transcript increased by both poly(I:C)- and flagellin-EVs. These transcript profiles support the idea of divergent, tailored responses of antigen presenting cells to PAMP-exposed keratinocyte EVs.

To confirm the array findings, we used probe-based qPCR to independently assess levels of the five transcripts significantly elevated by HFK EVs. BMP6, CXCL8 and VEGFA were significantly selectively upregulated by either poly(I:C)- or flagellin-EVs (Table 1). A 2.6-fold increase of CCL3 transcript was found after flagellin-EV stimulation but missed significance ($p = 0.076$). While our arrays found CXCL16 significantly upregulated 3.1-fold by poly(I:C)-EVs, our confirmation failed to detect upregulation over 2-fold. We also measured the effect the EVs had on *PTGS2* and *IL36γ* transcript levels, whose gene products are relevant to epithelial immune responses and not included on the qPCR arrays. Interestingly, *PTGS2* transcript, the gene encoding cyclooxygenase-2 (COX-2) was significantly up-regulated by flagellin-EVs but remained at baseline after stimulation with poly(I:C)-EVs and control-EVs (Fig. 5e). *IL36γ* mRNA was below detectable levels under all conditions (data not shown). Table 1 summarizes the significant changes in cytokine/chemokine transcripts along with expected functionality within epithelia.

4. Discussion

The functional effects of keratinocyte derived EVs on the host immune response are poorly understood. In this study, we have shown that unique sub-populations of EVs, with differences in their cargos, are generated when keratinocytes are stimulated with two different pathogen mimics. We have also concluded that the resulting keratinocyte EV population can potentially contribute to local immunomodulation by inducing changes in specific cytokine and chemokine transcripts in recipient antigen-presenting cells.

Our data supports the genesis of an unconventional EV population possessing biological and physical properties of EVs derived from both MVBs (exosomes) and autophagosomes during keratinocyte responses to poly(I:C). The secretion of the leaderless protein α-synuclein increased within a distinct sub-population of EVs that were described as having a hybrid "autophagosome-exosome-like profile" which were positive for both LC3A and LC3B when autophagy was altered in neurons modeling Parkinson's disease [20]. Secretion of annexin A2 within EVs from lung epithelial cells has been shown to be dependent on autophagy triggered by IFN-γ signaling, also providing a connection between selective EV biogenesis and pathogen response [15]. Our data strongly suggests that autophagy plays a role in the generation of specific EV subpopulations during the innate response of primary keratinocytes to some PAMPs but not others since EV properties, including cargo incorporation, diverge following poly(I:C) and flagellin stimulations.

Cellular responses to PAMPs, here exemplified by well-established TLR agonists poly(I:C) and flagellin, lead to changes in EV cargos and

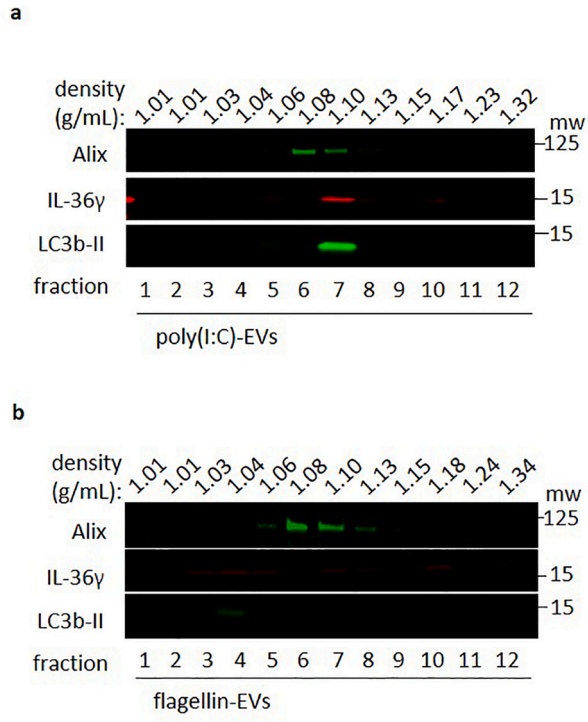

Fig. 3. TLR-3 simulation, but not TLR-5 stimulation leads to the release of a sub-population of IL36γ^{+}/LC3b-II^{+} EVs with the density of exosomes. Western blot of fractions derived from density gradient ultracentrifugation of EV pellets derived from 48-h poly(I:C)-treated (a) and flagellin-treated (b) HFK-conditioned media. Blots probed for EV markers Alix and LC3b-II and IL-36γ cargo. Representative of 3 experiments. mw: molecular weight, EVs: extracellular vesicles.

function [14,49,50]. We demonstrated that these changes in EVs may influence the innate epithelial immune responses via interactions with local antigen presenting cells. The pattern of cytokines induced in iLCs by EVs from poly(I:C)-stimulated, and flagellin-stimulated keratinocytes are clearly distinct and have characteristics of either anti-viral or anti-bacterial responses respectively. *BMP-6*, upregulated in iLCs only after incubation with poly(I:C)-EVs, induces interferon-stimulated genes, down-regulates *USP18* (a suppressor of interferon signaling) and induces an immediate exit from the cell cycle in epithelial stem cells, all favorable conditions during viral challenge [33,36]. In contrast, flagellin-EVs induced *CXCL8*, a chemotactic factor for neutrophils, a population of immunocytes primed to deal with bacterial pathogens while stimulating neutrophil degranulation and phagocytosis [37,51]. The robust, selective induction of *PTGS2* by flagellin-EVs is interesting but no conclusions can be drawn as to its role in cellular communication between HFKs and iLCs in this context. The gene product of *PTGS2,* COX-2, turns over Arachidonic acid into many leukotrienes and prostaglandins with pleiotropic effects of inflammation within epithelia [44]. It may be that COX-2 products, including PGE_2, are important for mounting or initiating an anti-bacterial response. Recent work demonstrates that PGE_2 inhibits NETosis of infiltrating neutrophils indicating a potential later, regulatory function for induced COX-2 [44]. Further studies are needed to describe the role of COX-2 in EV mediated cellular communication.

In this study, we have shown for the first time that treatment of keratinocytes with viral or bacterial PAMPs can induce alternate EV biogenesis and the subsequent immunomodulation, via EV crosstalk, of innate immune cells that would be expected to occur during the immediate stages of a viral vs. bacterial infection. There are however limitations to our study. Our in vitro functional studies may differ from in vivo responses. Potential immunomodulation by other factors present in the microenvironment (i.e. cytokines, other PAMPs) could affect LC responses to keratinocyte EVs. Additionally, with current techniques it is extremely difficult to assess the amounts of EVs and rates of interactions with APCs in an open system (i.e. epithelial tissues) to replicate them in vitro. We used a dose of EVs that would approximate those released from keratinocytes in proportion to the number of target iLCs [31]. However, even within the tissue itself, keratinocytes within close proximity to iLCs should deliver EVs at higher concentrations than those further away.

Future work will be needed to determine whether the larger EVs we visualized in the poly(I:C)-EVs are those that are LC3b-II^{+}, are truly derived from autophagosomes and whether the immunologic responses induced by the poly(I:C)-EVs are an effect of their potential autophagosomal origin, the presence of IL-36γ or a combination. Whether IL-36γ

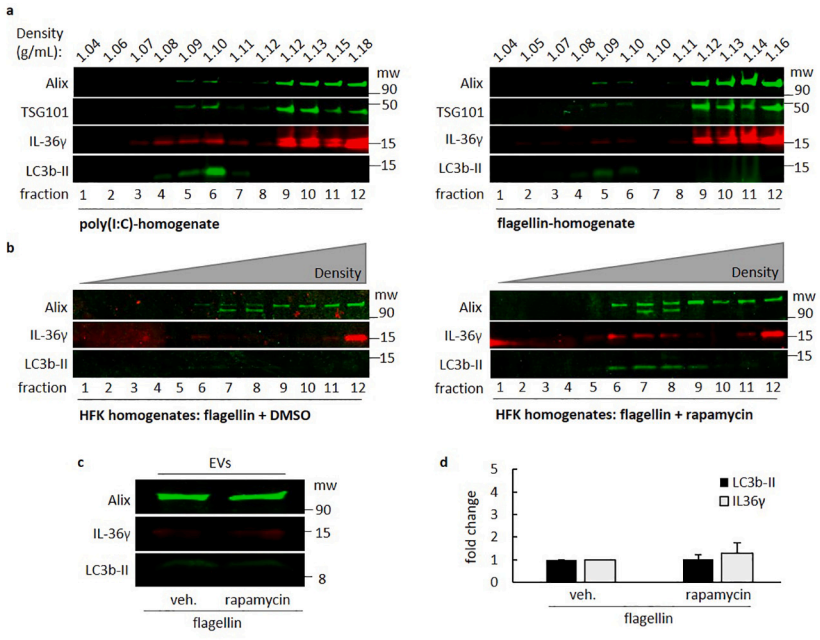

Fig. 4. Intracellular LC3b-II^{+} organelles track with IL-36γ during subcellular fractionation after poly(I:C) stimulation and induction of autophagy via rapamycin induces formation of LC3b-II^{+}/IL-36γ^{+} organelles. (a) Western blot of homogenates from HFKs stimulated for 24-h with poly(I:C) or flagellin and fractionated by density gradient centrifugation probing for EV markers Alix, TSG101, LC3b-II and IL-36γ cargo. Representative of 3 experiments. (b) Western blot of density gradient fractionated HFK homogenates 48 h after flagellin + vehicle control and flagellin + rapamycin co-stimulation probing for EV markers Alix, LC3b-II and IL-36γ cargo. Representative of 3 experiments. Fractionation was performed with equivalent masses of homogenates and blots were probed and visualized in parallel with equal exposures for comparison. (c) Western blot of total EV pellets derived from conditioned medium from flagellin + vehicle control or flagellin + rapamycin co-stimulation rapamycin and flagellin co-stimulated HFKs. (d) Quantification of EV associated LC3b-II and IL-36γ during rapamycin and flagellin co-stimulation. Intensity was normalized to Alix and expressed as fold change relative to DMSO controls. Bars represent mean ± SD of 3 experiments. mw: molecular weight, EV: extracellular vesicles, veh: vehicle control.

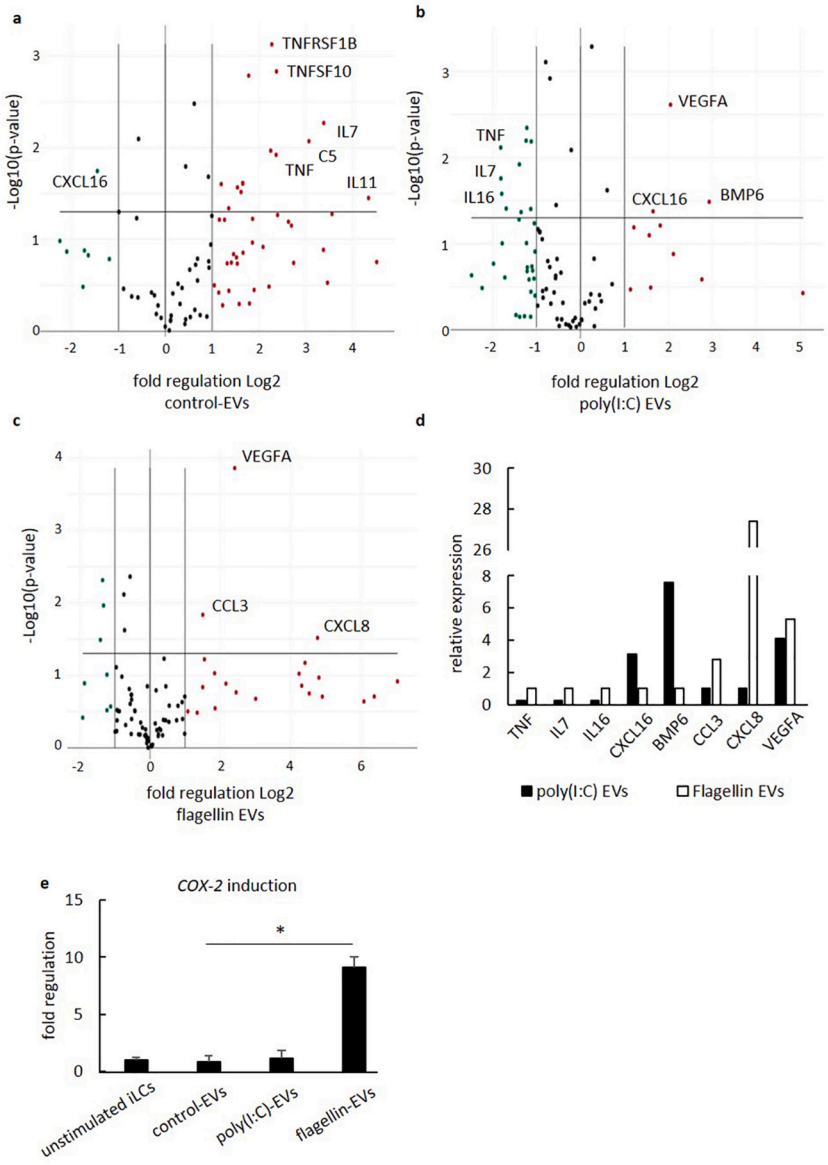

Fig. 5. Extracellular vesicles derived from poly(I:C)- and flagellin-stimulated human keratinocytes induce divergent cytokine/chemokine profiles in monocyte-derived Langerhans cells. Monocyte derived Langerhans cells (iLCs) were incubated with EVs from keratinocytes stimulated with poly(I:C) or flagellin or EVs from unstimulated keratinocytes. Cytokine/chemokine transcripts were measured using RT^2 qPCR profiler arrays (Qiagen). a-c) Volcano plots for the linearized change in cytokine/chemokine transcripts in iLCs, comparing a) unstimulated EVs vs. untreated iLCs without EVs; b) poly(I:C)-EVs vs. control-EVs; c) flagellin-EVs vs. control-EVs. Genes falling above the horizontal axis reached significance ($p < 0.05$) according to Students' *t*-tests. Labeled genes represent those expressed at meaningful levels. d) Relative levels of cytokines/chemokines whose mean expression was significantly altered when iLCs were incubated with EVs from TLR3- and TLR5-stimulated keratinocytes, compared to EVs from unstimulated keratinocytes. e) Induction of *PTGS2* (COX-2) in iLCs by HFK derived EVs as measured by qRT-PCR. Bars represent mean fold change ± SD in transcriptional levels of monocyte derived iLCs from 3 healthy donors, expressed relative to GAPDH, *p < 0.05 with Student's *t*-test. EVs: extracellular vesicles, TNF: Tumor Necrosis Factor, IL7: Interleukin-7, IL16: Interleukin-16, CXCL16: C-X-C Motif Chemokine Ligand 16, BMP6: Bone Morphogenetic Protein 6, CCL3: C—C Motif Chemokine Ligand 3, CXCL8: C-X-C Motif Chemokine Ligand 8, VEGFA: Vascular Endothelial Growth Factor A.

Table 1
Effects of EVs from TLR-stimulated HFKs on immune regulatory gene transcripts in Langerhans Cells.

Gene	Fold Change	p-value	Functions in Epithelial Tissues
poly(I:C)-EVs			
BMP6	6.09	0.001	Suppresses proliferation and induces terminal differentiation in keratinocytes (KCs) [33–35]. Regulates genes similar to those induced by interferon [36].
flagellin-EVs			
CXCL8	24.19	0.005	Strongly chemotactic for and activates neutrophils [37–40]. Secreted by flagellin-stimulated monocytes, T-cells and KCs [41–43].
PTGS2	9.00	0.020	Synthesis of a broad collection of bioactive prostaglandins [44]. Products of COX-2 enzyme have diverse effects on immunocytes that are largely context dependent [45,46].
VEGFA	3.52	0.018	Wound healing and angiogenesis [47]. Increases vascular permeability [48].

Gene transcripts significantly altered in iLCs by poly(I:C)- or flagellin-stimulated HFK derived EVs compared to control-HFK EVs. Transcripts were measured using probe-based qPCR and normalized to GAPDH. *p*-values were calculated by two-tailed, paired, Student's t-test. *BMP6*: Bone Morphogenetic Protein 6; *CXCL8*: C-X-C Motif Chemokine Ligand 8; PTG*S2:* Prostaglandin-endoperoxide synthase 2; *VEGFA*: Vascular Endothelial Growth Factor; KC: keratinocytes.

secreted in this manner has any impact on keratinocytes and surrounding APCs is currently unknown. Flagellin-EVs clearly induced significantly different responses in our iLC model compared to control-EVs, without major changes to EV size distribution, marker levels or density, indicating that these functional effects may stem from either more subtle alterations in the EV structures or the cargos they contain. Furthering our understanding of how EVs contribute to innate immune responses at epithelial surfaces will work toward completing the picture of cellular communication.

5. Conclusions

From this work, we have found that: 1) Normal keratinocytes respond to pathogen associated molecular patterns by altering the biogenesis and release of extracellular vesicles containing selective signaling molecules, including the cytokine IL-36γ, 2) Poly(I:C) stimulation leads to the release of a sub-population of EVs, likely derived from the autophagosome, and 3) EVs from poly(I:C) and flagellin-stimulated keratinocytes lead to significant, divergent transcriptional cytokine profiles in antigen presenting cells.

Supplementary data to this article can be found online at https://doi.org/10.1016/j.cellsig.2021.109994.

Declaration of Competing Interest

The authors report no conflict of interest.

Acknowledgments

The authors would like to thank Drs. Michael Bukrinsky, Lionel Blanc and Betsy J. Barnes for their valuable advice on this project and with interpreting EV functional data. This work was supported in part by the National Institutes of Dental and Craniofacial Research of the National Institutes of Health. United States of America. Award Number DE017227.

References

[1] J.A. Westrich, C.J. Warren, D. Pyeon, Evasion of host immune defenses by human papillomavirus, Virus Res. 231 (2017) 21–33.
[2] J. Hesse-Macabata, et al., Innate immune response of human epidermal keratinocytes and dermal fibroblasts to in vitro incubation of Trichophyton benhamiae DSM 6916, J. Eur. Acad. Dermatol. Venereol. 33 (2019) 1177–1188.
[3] M. Israr, et al., Microarray analysis of human keratinocytes from different anatomic sites reveals site-specific immune signaling and responses to human papillomavirus type 16 transfection, Mol. Med. 24 (2018) 23.
[4] A.I. Kajita, et al., Interferon-gamma enhances TLR3 expression and anti-viral activity in keratinocytes, J Invest Dermatol 135 (2015) 2005–2011.
[5] G. Kollisch, et al., Various members of the toll-like receptor family contribute to the innate immune response of human epidermal keratinocytes, Immunology 114 (2005) 531–541.
[6] R. Karim, et al., Human papillomavirus (HPV) upregulates the cellular deubiquitinase UCHL1 to suppress the keratinocyte's innate immune response, PLoS Pathog. 9 (2013), e1003384.
[7] Y.S. Ryu, et al., Particulate matter induces inflammatory cytokine production via activation of NFkappaB by TLR5-NOX4-ROS signaling in human skin keratinocyte and mouse skin, Redox Biol. 21 (2019) 101080.
[8] Z. Jiang, et al., IL-36gamma induced by the TLR3-SLUG-VDR Axis promotes wound healing via REG3A, J Invest Dermatol 137 (2017) 2620–2629.
[9] C. Jiang, et al., Treponema pallidum flagellins stimulate MMP-9 and MMP-13 expression via TLR5 and MAPK/NF-kappaB signaling pathways in human epidermal keratinocytes, Exp. Cell Res. 361 (2017) 46–55.
[10] M. Mathieu, L. Martin-Jaular, G. Lavieu, C. Thery, Specificities of secretion and uptake of exosomes and other extracellular vesicles for cell-to-cell communication, Nat. Cell Biol. 21 (2019) 9–17.
[11] G. van Niel, G. D'Angelo, G. Raposo, Shedding light on the cell biology of extracellular vesicles, Nat. Rev. Mol. Cell Biol. 19 (2018) 213–228.
[12] Y.S. Gho, C. Lee, Emergent properties of extracellular vesicles: a holistic approach to decode the complexity of intercellular communication networks, Mol. BioSyst. 13 (2017) 1291–1296.
[13] L. Paolini, A. Zendrini, A. Radeghieri, Biophysical properties of extracellular vesicles in diagnostics, Biomark. Med 12 (2018) 383–391.
[14] W. Fitzgerald, et al., A system of cytokines encapsulated in ExtraCellular vesicles, Sci. Rep. 8 (2018) 8973.
[15] Y.D. Chen, et al., Exophagy of annexin A2 via RAB11, RAB8A and RAB27A in IFN-gamma-stimulated lung epithelial cells, Sci. Rep. 7 (2017) 5676.
[16] A.A. Rana, et al., Poly(I:C) induces controlled release of IL-36gamma from keratinocytes in the absence of cell death, Immunol. Res. 63 (2015) 228–235.
[17] P.T. Walsh, P.G. Fallon, The emergence of the IL-36 cytokine family as novel targets for inflammatory diseases, Ann. N. Y. Acad. Sci. 1417 (2018) 23–34.
[18] E.Y. Bassoy, J.E. Towne, C. Gabay, Regulation and function of interleukin-36 cytokines, Immunol. Rev. 281 (2018) 169–178.
[19] M.A. Boutet, et al., Distinct expression of interleukin (IL)-36alpha, beta and gamma, their antagonist IL-36Ra and IL-38 in psoriasis, rheumatoid arthritis and Crohn's disease, Clin. Exp. Immunol. 184 (2016) 159–173.
[20] G. Minakaki, et al., Autophagy inhibition promotes SNCA/alpha-synuclein release and transfer via extracellular vesicles with a hybrid autophagosome-exosome-like phenotype, Autophagy 14 (2018) 98–119.
[21] D.K. Jeppesen, et al., Reassessment of Exosome Composition, Cell **177** (2019) 428–445, e418.
[22] J. Wu, et al., Molecular cloning and characterization of rat LC3A and LC3B–two novel markers of autophagosome, Biochem. Biophys. Res. Commun. 339 (2006) 437–442.
[23] D.J. Klionsky, et al., Guidelines for the use and interpretation of assays for monitoring autophagy (3rd edition), Autophagy 12 (2016) 1–222.
[24] C.M. Fader, M.I. Colombo, Autophagy and multivesicular bodies: two closely related partners, Cell Death Differ. 16 (2009) 70–78.
[25] J. Lin, et al., Cross-regulation between exosomal and autophagic pathways: promising therapy targets in disease, Discov. Med. 27 (2019) 201–210.
[26] J. Tian, et al., Interplay between Exosomes and autophagy in cardiovascular diseases: novel promising target for diagnostic and therapeutic application, Aging Dis. 10 (2019) 1302–1310.
[27] B.W. Darbro, G.B. Schneider, A.J. Klingelhutz, Co-regulation of p16INK4A and migratory genes in culture conditions that lead to premature senescence in human keratinocytes, J Invest Dermatol 125 (2005) 499–509.
[28] C. Thery, S. Amigorena, G. Raposo, A. Clayton, Isolation and characterization of exosomes from cell culture supernatants and biological fluids, Curr Protoc Cell Biol 22 (2006). **Chapter 3**, Unit 3.
[29] J. DeVoti, et al., Decreased Langerhans cell responses to IL-36gamma: altered innate immunity in patients with recurrent respiratory papillomatosis, Mol. Med. 20 (2014) 372–380.
[30] M. Israr, et al., Altered monocyte and Langerhans cell innate immunity in patients with recurrent respiratory Papillomatosis (RRP), Front. Immunol. 11 (2020) 336.
[31] J. Bauer, et al., A strikingly constant ratio exists between Langerhans cells and other epidermal cells in human skin. A stereologic study using the optical disector method and the confocal laser scanning microscope, J Invest Dermatol 116 (2001) 313–318.
[32] J. Kowal, et al., Proteomic comparison defines novel markers to characterize heterogeneous populations of extracellular vesicle subtypes, Proc. Natl. Acad. Sci. U. S. A. 113 (2016) E968–E977.
[33] F.P. Gosselet, T. Magnaldo, R.M. Culerrier, A. Sarasin, J.C. Ehrhart, BMP2 and BMP6 control p57(Kip2) expression and cell growth arrest/terminal differentiation in normal primary human epidermal keratinocytes, Cell. Signal. 19 (2007) 731–739.
[34] J.H. Kim, et al., HIF-1alpha-mediated BMP6 down-regulation leads to hyperproliferation and abnormal differentiation of keratinocytes in vitro, Exp. Dermatol. 27 (2018) 1287–1293.
[35] M.A. Phillips, Q. Qin, Q. Hu, B. Zhao, R.H. Rice, Arsenite suppression of BMP signaling in human keratinocytes, Toxicol. Appl. Pharmacol. 269 (2013) 290–296.
[36] L.A. Eddowes, et al., Antiviral activity of bone morphogenetic proteins and activins, Nat. Microbiol. 4 (2019) 339–351.
[37] A. Vacchini, et al., Differential effects of posttranslational modifications of CXCL8/Interleukin-8 on CXCR1 and CXCR2 internalization and signaling properties, Int. J. Mol. Sci. **19** (2018).
[38] P.R.B. Joseph, K.V. Sawant, K. Rajarathnam, Heparin-bound chemokine CXCL8 monomer and dimer are impaired for CXCR1 and CXCR2 activation: implications for gradients and neutrophil trafficking, Open Biol. **7** (2017).
[39] T.K. Wright, et al., Neutrophil extracellular traps are associated with inflammation in chronic airway disease, Respirology 21 (2016) 467–475.
[40] S.T. Das, et al., Monomeric and dimeric CXCL8 are both essential for in vivo neutrophil recruitment, PLoS One 5 (2010), e11754.
[41] H.J. Metcalfe, R.M. La Ragione, D.G. Smith, D. Werling, Functional characterisation of bovine TLR5 indicates species-specific recognition of flagellin, Vet. Immunol. Immunopathol. 157 (2014) 197–205.
[42] A.S. Akhade, A. Qadri, T-cell receptor activation of human CD4(+) T cells shifts the innate TLR response from CXCL8(hi) IFN-gamma(null) to CXCL8(lo) IFN-gamma (hi), Eur. J. Immunol. 45 (2015) 2628–2637.
[43] C. Bannon, P.J. Davies, A. Collett, G. Warhurst, Potentiation of flagellin responses in gut epithelial cells by interferon-gamma is associated with STAT-independent regulation of MyD88 expression, Biochem. J. 423 (2009) 119–128.
[44] G.J. Martinez-Colon, B.B. Moore, Prostaglandin E2 as a regulator of immunity to pathogens, Pharmacol. Ther. 185 (2018) 135–146.
[45] W.H.S. Nasry, J.C. Rodriguez-Lecompte, C.K. Martin, Role of COX-2/PGE2 mediated inflammation in oral squamous cell carcinoma, Cancers (Basel) **10** (2018).
[46] N. Hashemi Goradel, M. Najafi, E. Salehi, B. Farhood, K. Mortezaee, Cyclooxygenase-2 in cancer: a review, J. Cell. Physiol. 234 (2019) 5683–5699.
[47] N.N. Nissen, et al., Vascular endothelial growth factor mediates angiogenic activity during the proliferative phase of wound healing, Am. J. Pathol. 152 (1998) 1445–1452.

[48] H.F. Dvorak, et al., Vascular permeability factor/vascular endothelial growth factor: an important mediator of angiogenesis in malignancy and inflammation, Int. Arch. Allergy Immunol. 107 (1995) 233–235.
[49] S. Bhatnagar, K. Shinagawa, F.J. Castellino, J.S. Schorey, Exosomes released from macrophages infected with intracellular pathogens stimulate a proinflammatory response in vitro and in vivo, Blood 110 (2007) 3234–3244.
[50] T. Kouwaki, M. Okamoto, H. Tsukamoto, Y. Fukushima, H. Oshiumi, Extracellular vesicles deliver host and virus rna and regulate innate immune response, Int. J. Mol. Sci. **18** (2017).
[51] M. Metzemaekers, S. Vandendriessche, N. Berghmans, M. Gouwy, P. Proost, Truncation of CXCL8 to CXCL8(9-77) enhances actin polymerization and in vivo migration of neutrophils, J. Leukoc. Biol. 107 (2020) 1167–1173.